

INTERGALACTIC SHOCK FRONTS

MAXIM MARKEVITCH

*Harvard-Smithsonian Center for Astrophysics,
60 Garden St., Cambridge, MA 02138, USA*

Review talk at 12th Marcel Grossman Meeting, Paris, July 2009 (updated with 2010 results)

When galaxy clusters collide, they generate shock fronts in the hot intracluster medium. Observations of these shocks can provide valuable information on the merger dynamics and physical conditions in the cluster plasma, and even help constrain the nature of dark matter. To study shock fronts, one needs an X-ray telescope with high angular resolution (such as *Chandra*), and be lucky to see the merger from the right angle and at the right moment. As of this writing, only a handful of merger shock fronts have been discovered and confirmed using both X-ray imaging and gas temperature data — those in 1E 0657–56, A520, A754, and two fronts in A2146. A few more are probable shocks awaiting temperature profile confirmation — those in A521, RXJ 1314–25, A3667, A2744, and Coma. The highest Mach number is 3 in 1E 0657–56, while the rest has $M \simeq 1.6–2$. Interestingly, all these relatively weak X-ray shocks coincide with sharp edges in their host cluster’s synchrotron radio halos (except in A3667, where it coincides with the distinct radio relic, and A2146, which does not have radio data yet). This is contrary to the common wisdom that weak shocks are inefficient particle accelerators, and may shed light on the mechanisms of relativistic electron production in astrophysical plasmas.

Keywords: Galaxy clusters; Intergalactic medium; Shock fronts; Dark matter; Cosmic rays

1. Introduction

Mergers of galaxy clusters provide a unique laboratory to study the cluster physics — they generate shocks, hydrodynamic instabilities and turbulence in the hot intracluster medium (ICM). They also cause “cold fronts”, or contact discontinuities, around the cores of infalling subclusters or in the disturbed cool core of the main cluster.¹ In turn, these ICM disturbances distort and amplify magnetic fields (which are frozen into the ICM) and generate ultrarelativistic electrons that produce diffuse synchrotron emission of cluster-wide radio halos.^{2–4} Of these phenomena, with the current instruments, we can directly observe shock fronts and cold fronts as sharp brightness and temperature edges in high angular resolution X-ray images — Fig. 1 shows a poster child of the merger shocks, the “bullet cluster” 1E 0657–56,^{5–7} and Fig. 2 shows a cold front in the “cannonball galaxy” NGC 1404.⁸ In the radio, the synchrotron emission is a product of density of ultrarelativistic electrons and B^2 , where the magnetic field B is deduced by indirect means.⁹ Disentangling the relativistic electron density and the magnetic field (e.g., by observing inverse Compton emission from the radio halos), as well as direct observation of turbulence in the ICM, are beyond the current observing capabilities.

Figure 3 schematically shows the ICM density, pressure and specific entropy profiles in a sector in front of the “bullet” in the Bullet cluster. The sector crosses a cold front (the boundary of the bullet) and the shock that propagates ahead of it (Fig. 1). While both these X-ray brightness edges exhibit similar density jumps,

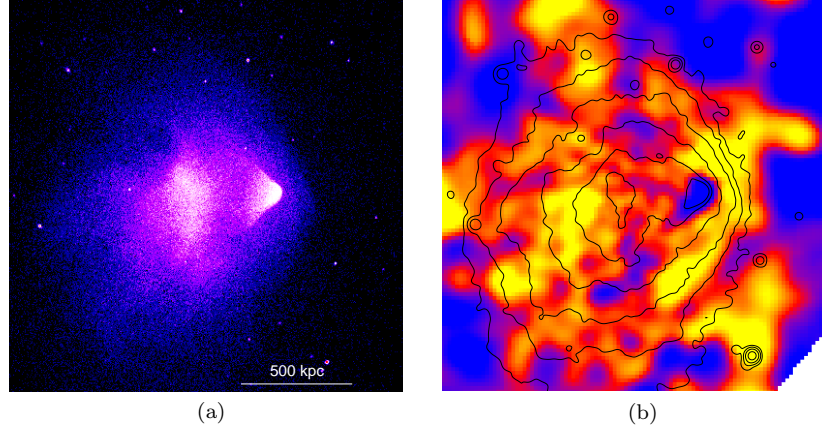


Fig. 1. The Bullet cluster 1E0657-56. (a) *Chandra* X-ray image (0.8-4 keV band, 7' size), (b) gas temperature map (color; blue is $T < 6$ keV and yellow is $T > 20$ keV) and X-ray brightness (contours). A cool gas bullet is preceded by a hot shock front.

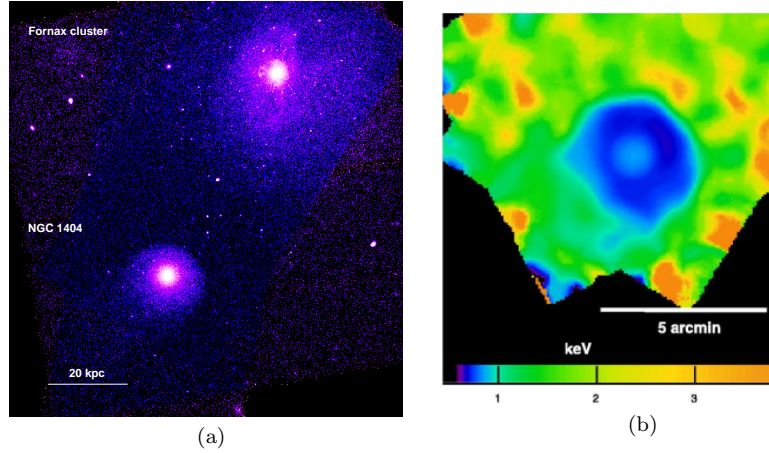


Fig. 2. Elliptical galaxy NGC 1404 falling toward the center of the Fornax cluster. (a) *Chandra* X-ray image (0.5-2 keV band, 17' size), (b) gas temperature map⁸ (a zoom-in on NGC 1404). The sharp NW boundary of the galaxy is a cold front.

the pressure across the cold front is almost continuous, as expected for a contact discontinuity between the dense, low-entropy remnant of an infalling subcluster and the surrounding shock-heated gas. The shock front exhibits a large pressure jump and a modest entropy increase, corresponding to its relatively low Mach number, $M = 3$.

Cold fronts are more easily observable than shock fronts – they were first discovered with *Chandra* in a merging cluster A2142¹⁰ and subsequently observed in most mergers. More surprisingly, they are also seen in the cool cores of at least half

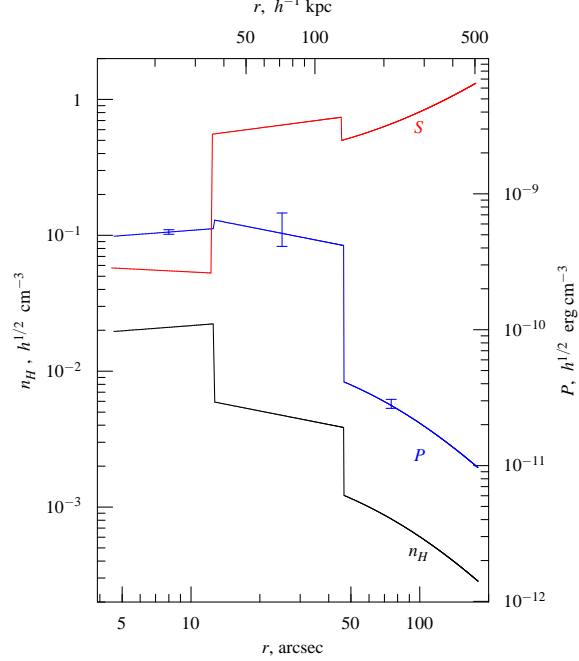


Fig. 3. Schematic gas density, pressure and specific entropy profiles in a sector of the Bullet cluster crossing the bullet nose and the shock front. The density jump around $r = 12''$ is a cold front (the front boundary of the gas bullet), and the jump at $r = 50''$ is a shock front.

of all relaxed clusters.^{1,11} Merger shock fronts quickly move away from the central, bright cluster regions into the faint outskirts, where they are difficult to observe in X-rays. To be discernible in an X-ray image, they also require a merger to occur almost exactly in the plane of the sky. For these reasons, only a handful is currently known, and they are the subject of this review. There are other types of shock fronts expected in clusters — far in the outskirts, a strong shock should separate the virialized cluster region and the outside infalling matter, but the X-ray brightness at those distances is far too low for these shocks to be observable at present. Explosions of the central AGNs also generate shocks in the cluster cores, usually with $M \approx 1$, but sometimes much stronger.¹² These shocks are outside the scope of this review.

2. Constraints on dark matter from the Bullet cluster

We will start with some physical results already derived using the most prominent cluster shock front, the one in the Bullet cluster 1E0657–56. Fig. 1 shows an X-ray image and projected temperature map derived from a 500 ks *Chandra* exposure^{7,13,14} of 1E0657–56, and Fig. 4 overlays a weak lensing total mass map¹⁶ on the *Chandra* image. It is clear from these figures that 1E0657–56 is a merger

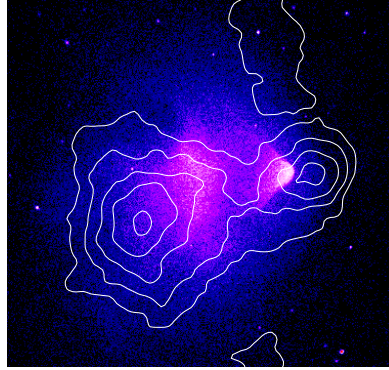


Fig. 4. X-ray image of 1E0657-56 (same as in Fig. 1a) with contours showing total projected mass from weak lensing. The gas subcluster trails its mass peak because of ram pressure. This offset is direct proof of the existence of dark matter.¹⁶

of two subclusters flying apart just after a collision. The cooler gas bullet, with its characteristic shuttlecock shape, appears to be a remnant of the cool core of the smaller subcluster, pushed back from its host dark matter peak by ram pressure. The X-ray brightness and temperature profiles across the shock front give a Mach number ($M = 3.0 \pm 0.4$) and a velocity of the shock front (4700 km s^{-1}).⁶ The velocity of the subcluster is probably lower than that of the shock front, because the pre-shock gas flows in from the cluster outskirts toward the shock front under the gravitational pull of the subcluster.¹⁷ The two subclusters should have passed through each other just 200 million years ago.

It has been quickly realized^{15,16} that the offset between the peaks of the total mass and the gas mass peaks seen in Fig. 4 offers the first direct and model-independent evidence for the existence of dark matter, as opposed to some forms of modified gravity, where the visible matter is all there is and the laws of gravity are incorrect on large scales^{18,19} — an alternative possibility put forward to explain the longstanding problem of “missing mass” in galaxy clusters.²⁰ Indeed, the X-ray emitting gas is by far the dominant visible mass component in clusters, and yet, as the lensing mass map shows, the peaks of the *total* mass density are clearly located elsewhere. The measured total masses in those peaks are as expected from the ratio of gas mass, stellar mass in the galaxies, and total mass normally observed in clusters. What makes this cluster unique is the moment at which it is caught by the observer — when gas and dark matter have been temporarily spatially separated by a violent merger, revealing that these are indeed two different kinds of matter.

The survival of two dark matter subclusters after a near-direct collision (indicated by the X-ray data) also provides an upper limit on self-interaction cross-section for the dark matter particles. The dark matter peaks coincide with peaks of the galaxy number density, and both dark matter and galaxy peaks are located ahead of the gas, as expected for collisionless dark matter and galaxies vs.

fluid-like ICM. The observed mass-to-light ratio within the gas-depleted subcluster peaks is found to be similar to that in other clusters within similar radii. This excludes the possibility that a significant fraction of dark matter particles has escaped the subclusters as a result of particle collisions during the subclusters' recent passage through each other. Taking into account the merger velocity derived from the X-ray, this observation places a limit of $\sigma/m < 0.7 \text{ cm}^2/\text{g}$ on the dark matter self-interaction cross-section,^{21,22} excluding most of the astrophysically interesting range of the cross-section.²³

3. Electron-proton equilibration timescale in the ICM

The passage of a merger shock in a fully ionized intracluster plasma should heat the protons dissipatively, while electrons (for shocks with $M \ll (m_p/m_e)^{1/2} \approx 43$, which is always true for cluster mergers) are compressed adiabatically and subsequently heated by other mechanisms, such as Coulomb collisions with hotter protons. The linear sizes and temperatures of galaxy clusters are such that on a timescale of collisional electron-proton equilibration, τ_{ep} , the shock travels significant distances, creating observable regions where the electron temperature T_e (the only one that we can currently measure in X-rays) is below the true thermodynamic temperature. This is illustrated in Fig. 5, which shows simulated maps of the average and electron temperatures for a merging cluster with two shocks propagating outwards, assuming collisional τ_{ep} . The T_e/T_p nonequilibrium is expected in many types of astrophysical objects, from solar wind to supernovae to WHIM filaments. However,

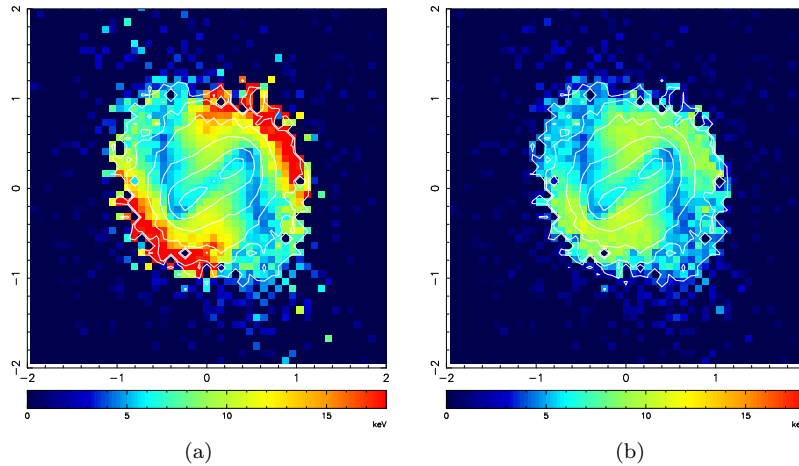


Fig. 5. Simulations of a cluster merger,²⁴ with colors showing the temperature and contours showing the mass. There are two shock fronts propagating ahead of two subclusters that have just crossed each other. (a) Average plasma temperature, (b) electron temperature assuming Coulomb electron-proton equilibration timescale. The linear scale is in Mpc and the temperature scale is in keV. The X-ray measured T_e may be a significant underestimate of thermodynamic temperature at shocks.

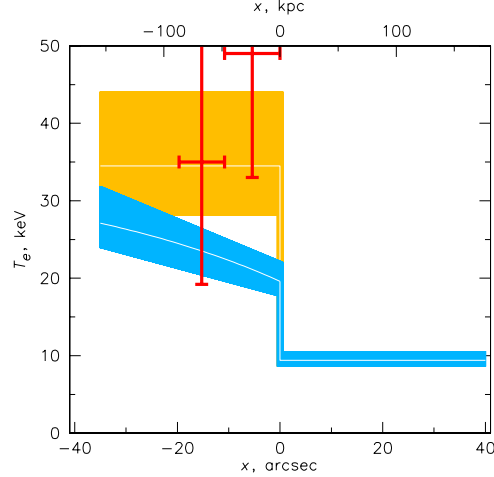


Fig. 6. Predicted T_e profiles for the shock in 1E0657–56, for the Coulomb electron-proton equilibration timescale (blue band) and for instant equilibration (yellow band). Overlaid is the *Chandra* measurement (deprojected, with 1σ error bars), which indicate a shorter equilibration timescale.⁶

it is usually impossible to measure T_e and T_p independently *and* map them on linear scales on which their equilibrium is expected to be achieved. Shock fronts in clusters provide a unique opportunity to do so and thus constrain τ_{ep} . Because cluster shocks are relatively weak, the easily measurable plasma density jump at the shock is sufficiently far from its asymptotic value (factor of 4 for a $\gamma = 5/3$), which allows one to derive the Mach number of the shock from the density jump using the Rankine-Hugoniot jump conditions, and predict the equilibrium post-shock value of the plasma temperature independently of the measured jump in T_e . The pre-shock T_e gives the sound speed, which, together with the shock density jump, gives the speed of the post-shock gas flow relative to the shock front. This can be used to predict the post-shock T_e profile for various values of τ_{ep} . For the shock in 1E0657–56 with $M = 3$, the expected rise in post-shock T_e for the case of Coulomb collisions can be spatially resolved by *Chandra*, as shown in Fig. 6. The measured values of the post-shock T_e exclude the Coulomb timescale at a 95% significance, favoring a much shorter τ_{ep} .⁶

4. Other clusters with known shock fronts

Until recently, only two merger shock fronts were known and confirmed by the X-ray temperature measurement — the 1E0657–56 discussed above and A520 shown in Fig. 7a. The latter has a shock with $M \simeq 2$;²⁵ its recent long *Chandra* observation is currently being analyzed to validate the above constraint on τ_{ep} . A520 also exhibits a similar offset between gas and dark matter.²⁶

Recently, several more shock fronts and shock candidates were found in X-rays. A unique case of two fronts located on the opposite sides of the cluster has been

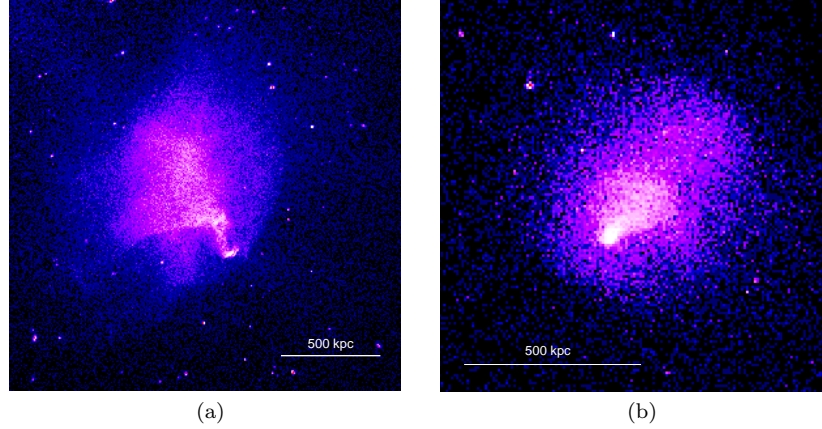


Fig. 7. (a) *Chandra* image of A520; the shock front with $M = 2$ is to the SW of the bright central structure.²⁵ (b) *Chandra* image of A2146, showing two $M \simeq 2$ shocks about 300 kpc SE and NW of the center.²⁷

reported in A2146,²⁷ shown in Fig. 7b — a geometry expected for a symmetric merger with a small impact parameter. Both shocks have $M \approx 2$. Similar second shocks are not observed in either 1E0657–56 or A520, most likely because those shocks have already moved out of the bright central regions in these mergers of subclusters of very different masses.

Now that we know how the merger shocks look like, it is possible to find them in archival X-ray data of lower quality. A possible shock front was detected in the *ROSAT* PSPC image of A754²⁸ and recently confirmed using the *Chandra* temperature measurement across the shock,³⁰ as shown in Fig. 8. This is a relatively weak shock with $M = 1.6$.

As of this writing (August 2010), these are the only known merger shocks with the X-ray temperature profiles confirming that an edge-like feature in the X-ray brightness is indeed a shock front (and not a cold front, for example). There are several other *likely* shock fronts seen in the X-ray images but awaiting temperature confirmation. One is in Coma cluster, seen in a *ROSAT* PSPC mosaic (Fig. 9). There is some indication of a temperature jump of the correct sign in the *XMM-Newton* temperature map,³¹ though a measurement more matched to the shock position is needed to verify this. Coma is big enough for this putative shock front to be seen by the *Planck* observatory that maps the Sunyaev-Zeldovich signal, which is proportional to gas pressure and thus should readily reveal shocks.

Another candidate front is found in the *Chandra* image of A2744, a spectacular merger at $z = 0.3$. An X-ray brightness profile in a sector containing the putative shock is shown in Fig. 10. The putative shock is a very low-contrast feature, likely corresponding to a low Mach number. We will see below that both Coma and A2744 exhibit edge features in their radio halo maps that coincide with these putative shocks.

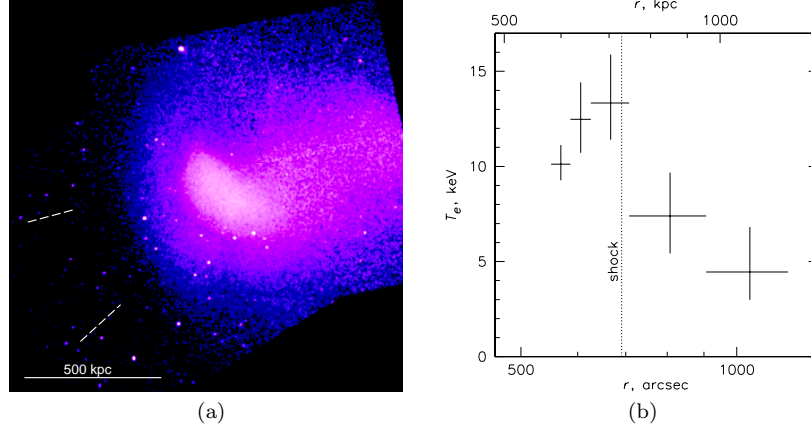


Fig. 8. (a) *Chandra* image of A754 with the sector showing a shock front with $M \simeq 1.6$.^{28,30} (b) *Chandra* gas temperature profile showing a temperature jump across the front in a sector shown in panel (a) (radius is from the shock's center of curvature), confirming that this is indeed a shock.³⁰

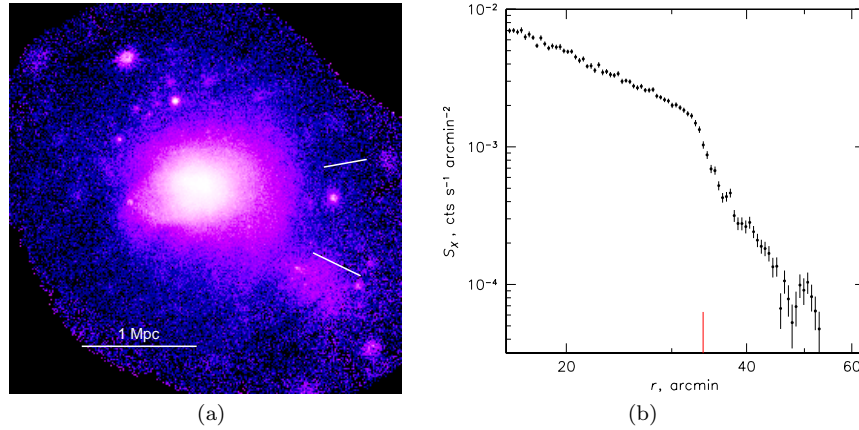


Fig. 9. (a) *ROSAT* PSPC mosaic of Coma ($1.6^\circ \times 1.6^\circ$), showing a brightness edge in the eastern sector (shown by dashes) that might be a shock front. (b) X-ray brightness profile in that sector, showing this feature at around $r = 33'$ (red dash).

It has long been suggested that peripheral radio relics are caused by electrons accelerated at shock fronts in the periphery of merging clusters.³² However, most relics are located far from the X-ray bright cluster regions, so it is rarely possible to check for the presence of a shock front in an X-ray image, and even more difficult to get a confirming temperature measurement.

A likely shock in A521 was discovered by analyzing the *Chandra* X-ray image at the position of a prominent radio relic,³³ see Fig. 11. There is a subtle X-ray brightness edge right where the “front” side of the relic is. The relic has a good radio spectrum, well represented by a power law. If one assumes that the radio-emitting

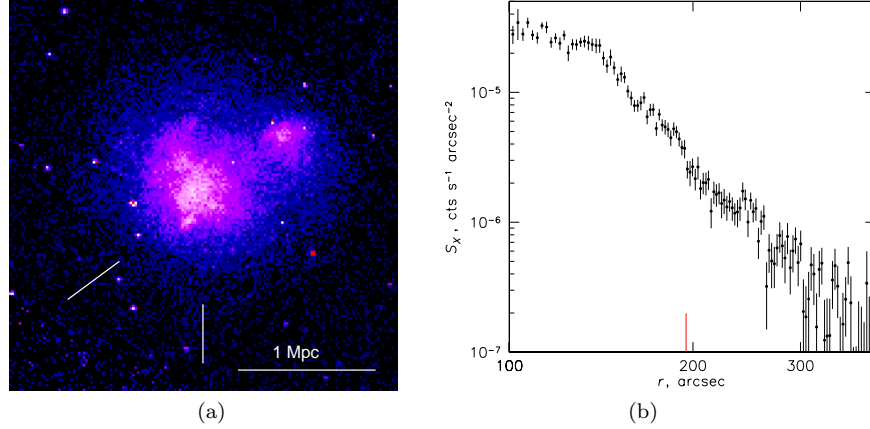


Fig. 10. (a) *Chandra* image of A2744 ($10' \times 10'$), showing a subtle brightness edge in the SE sector (shown by dashes) that might be a shock front. (b) X-ray brightness profile in that sector, showing this feature at around $r = 190''$ (red dash).

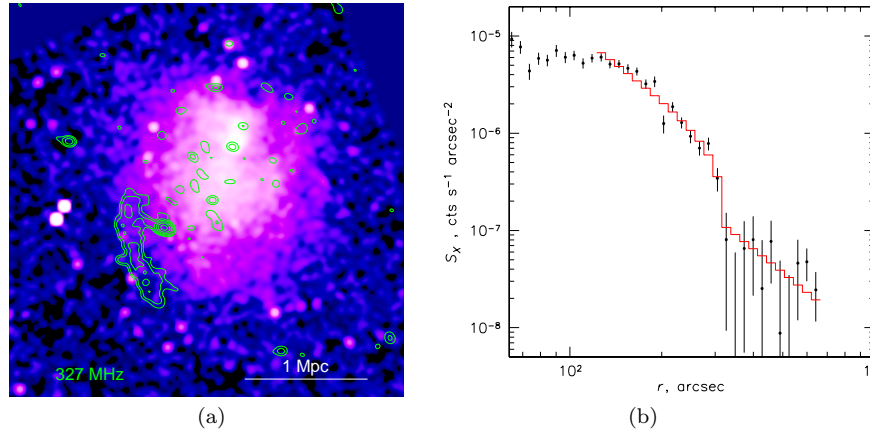


Fig. 11. (a) *Chandra* image of A521, with *GMRT* 327 MHz synchrotron radio relic contours overlaid,³³ delineating a possible shock front. (b) *Chandra* X-ray brightness profile in the sector covered by the relic; radius is from the relic's center of curvature. Overlaid is a model shock profile with $M = 2.3$ predicted from the radio spectrum of the relic,³³ which is consistent with the X-ray imaging data. Gas temperature data with sufficient quality is not yet available to confirm this shock.

relativistic electrons come from Fermi acceleration at the shock, the spectrum implies $M = 2.3$. The density jump for such a shock is in good agreement with the X-ray brightness profile, as shown by red model in Fig. 11b. At lower radio frequencies, this cluster reveals a giant radio halo that starts at the relic and spans the entire cluster⁴ (Fig. 12, discussed below).

An X-ray brightness edge that looks like a shock was discovered in an *XMM-Newton* observation of the famous NW radio relic in A3667;³⁵ if this is indeed a

shock, the gas density jump indicates $M \approx 2$. A possible $M \approx 2$ shock front was discovered at the position of a radio relic in the cluster RXJ 1314–25.³⁶ The curious M shape of this front indicates a velocity gradient in the pre-shock gas — possibly an extreme case of the effect seen in the hydrodynamic simulations of the Bullet cluster.¹⁷ Table 1 gives a summary of the currently known merger shocks.

Table 1. X-ray merger shock fronts and candidates (as of summer 2010)

Cluster	ρ jump	T jump	M	Radio edge?	X-ray refs.
1E 0657–56	yes	yes	3	yes	5,6
A520	yes	yes	2	yes	25
A754	yes	yes	1.6	yes	28–30
A2146 N	yes	yes	2	no data	27
A2146 S	yes	yes	2	no data	27
A521	yes		2	yes	33
RXJ 1314–25	yes		2	yes	36
A3667	yes		2	yes	35
A2744	yes			yes	this work
Coma	yes			yes	this work

5. Radio halos and X-ray shock fronts

Merger shock fronts are expected and, as we saw above, observed to have relatively low Mach numbers. Indeed, a test particle falling into the gravitational potential of a typical cluster would acquire $M \sim 3–4$. An infalling subcluster would generate multiple shocks in front of it, preheating the ambient gas and further reducing its Mach number by the time it arrives into the cluster’s X-ray bright central region, where we observe it. Such weak shocks are believed to be inefficient accelerators of electrons from the thermal pool to Lorentz factors $\sim 10^4$ required to produce relics and radio halos.^{30,37} Yet, it has been noticed that synchrotron radio halos in 1E 0657–56⁵ and A520²⁵ display brightness edges coincident with the X-ray shocks (Fig. 12), indicating that these shocks must have something to do with producing radio emission at least at those locations — either accelerating electrons, or compressing or re-accelerating a pre-existing relativistic electron population, and perhaps strengthening the magnetic fields beyond simple compression.²⁵ Re-acceleration of pre-existing relativistic electrons is an attractive theoretical possibility.^{38,39}

All the clusters with newly discovered X-ray shocks and shock candidates exhibit radio halos or relics, except A2146 that doesn’t have sensitive radio data yet. It is interesting to overlay the radio images on the X-ray shocks, which we do in Fig. 12. In addition to 1E 0657–56 and A520 discussed above, it shows A521, which exhibits a relic coincident with the probable shock, plus a halo extending from that relic across the whole cluster^{33,34} — a radio morphology very similar to A520. A754, with the weakest shock ($M = 1.6$), exhibits a steep-spectrum relic at 74 MHz,⁴⁰ coincident

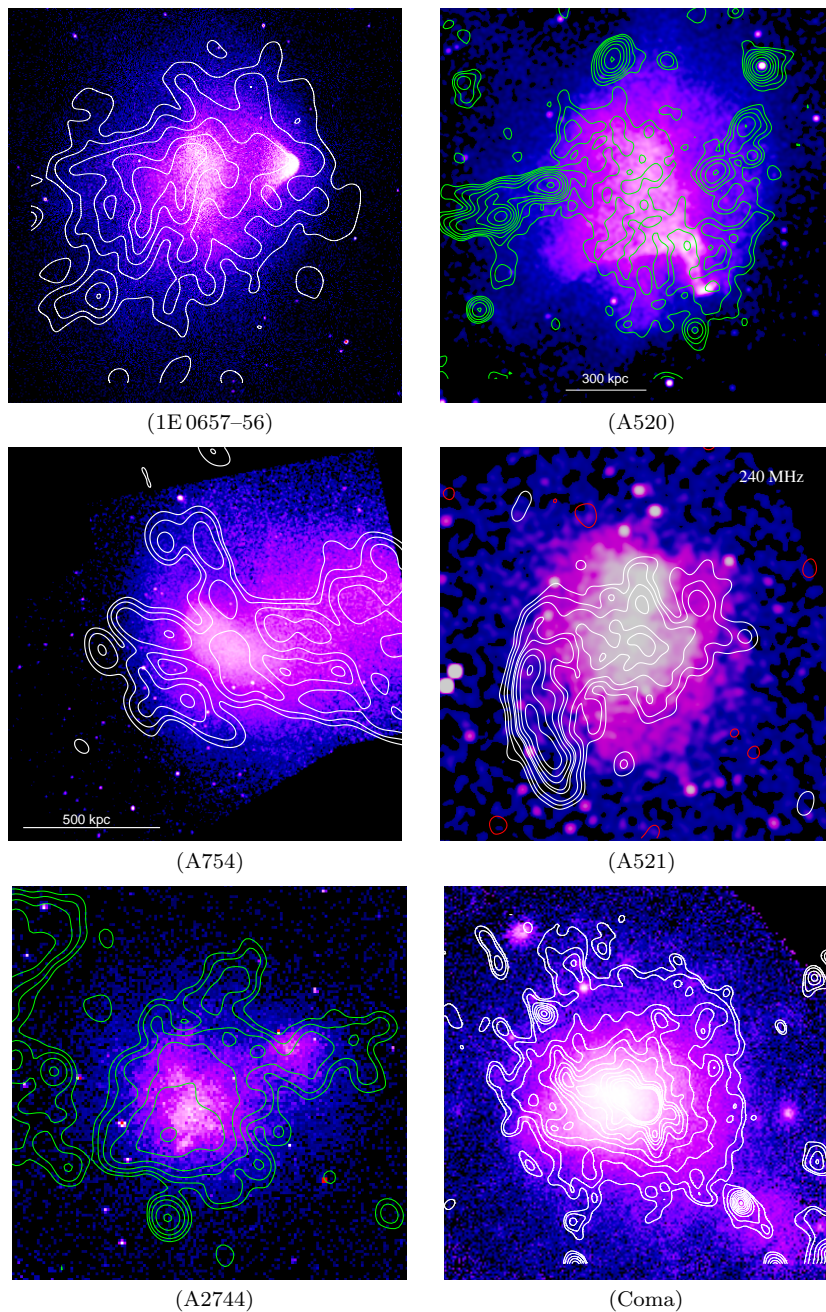


Fig. 12. Contours of radio halos overlaid on X-ray images of clusters with shock fronts (1E 0657-56,^{5,42} A520,^{25,43} A754³⁰) or front candidates (A521,³⁴ A2744,⁴⁴ Coma⁴⁵). In all cases, there is coincidence of a shock front seen in the X-ray with an edge in the radio halo.

with the shock front, and a radio halo extending from the relic westward across the cluster.^{30,41} Finally, the two shock candidates in A2744 and Coma, which we report in this paper, both have edge-like features seen in recent high-quality radio images of their halos,^{44,45} coincident with putative X-ray shock fronts. In Coma, the X-ray edge spans the southern half of the radio edge (Fig. 12). The cluster RXJ 1314–25 (not shown) also has a relic at the shock front and a small radio halo extending from it.³⁶

Thus, spatial coincidence of the merger shocks with edges of radio halos — or with radio relics that delineate an edge of the radio halo — is quite ubiquitous. It supports the scheme that we proposed for A520 and A521,³⁴ in which a weak merger shock re-accelerates pre-existing relativistic electrons (which may remain from earlier mergers, or generated by collisions of the long-lived cosmic ray protons with thermal protons⁴⁷). As these electrons move downstream from the shock, they rapidly cool, creating a narrow arc-like “relic”, but at a certain distance are picked up and re-accelerated again by turbulence generated by the merger behind the shock, which produces the cluster-wide halo. In this picture, the edge of the radio halo and the bulk of the halo are distinct phenomena, though both caused by the same merger. Depending on the Mach number of the shock, the magnetic field behind the shock (that determines the rate of synchrotron cooling of the electrons and thus the width of the “relic” in the direction across the shock front), and the power spectrum of turbulence in the body of the ICM behind the shock, the relic may appear at some frequencies as a distinct radio source, while at other frequencies, merge with the halo. In A521, the relic is dominant at $\nu > 1$ GHz, while in A754, the relic dominates at 74 MHz but merges with the halo at higher radio frequencies. The prediction of this picture is that the radio spectrum at the halo “edge” should be a power law determined by the shock’s Mach number (Fermi acceleration from thermal pool and re-acceleration from plausible initial electron distributions result in the same spectrum). This is again consistent with observations of A521³³ and A754.³⁰ The radio spectrum of the rest of the halo (more exactly, the frequency of its exponential cutoff) is determined by the velocity of the turbulence and the strength of the magnetic field.⁴⁶ Depending on that spectrum, it may or may not be possible to see the steepening of the radio spectrum of the front edge due to aging of electrons as one moves from the shock front inward (as was possible for A521³³).

We note that some more irregularly shaped cluster radio relics, such as a bright relic in A2744 (seen in the left edge of the image in Fig. 12), A2256 or A3667, may have different origin, perhaps involving a shock passage across a distinct region of fossil radio plasma.⁴⁸

It is clear that detailed, spatially resolved studies of cluster merger shocks in the X-ray and at multiple radio frequencies is a promising way to study the cosmic ray acceleration mechanisms in astrophysical plasmas. We may be starting to collect a sufficiently large sample for such studies.

References

1. M. Markevitch & A. Vikhlinin, *Phys. Reports*, 443, 1 (2007).
2. R. Cassano, in *The Low-Frequency Radio Universe*, ASP Conf. Series, 407, 223 (2009).
3. C. Sarazin, *JKAS*, 37, 433 (2004).
4. Brunetti, G., Cassano, R., Dolag, K., & Setti, G., *A&A*, 507, 661 (2009).
5. Markevitch, M., et al., *ApJ Lett.*, 567, L27 (2002).
6. Markevitch, M., in *The X-ray Universe 2005*, 604, 723 (2006).
7. Markevitch, M., et al., in preparation (2010).
8. Machacek, M., et al. *ApJ*, 621, 663 (2005).
9. Carilli, C. L. & Taylor, G. B. *ARAA*, 40, 319 (2002)
10. Markevitch, M., et al., *ApJ*, 541, 542 (2000).
11. Markevitch, M., Vikhlinin, A., Forman, W. R. in *Matter and Energy in Clusters of Galaxies*, ASP Conf. Series, 301, 37 (2003).
12. Croston, J. H., et al. *MNRAS*, 395, 1999 (2009).
13. Million, E. T., & Allen, S. W. *MNRAS*, 399, 1307 (2009).
14. Owers, M. S., Nulsen, P. E. J., Couch, W. J., & Markevitch, M. *ApJ*, 704, 1349 (2009).
15. Clowe, D., Gonzalez, A., & Markevitch, M. *ApJ*, 604, 596 (2004).
16. Clowe, D., Bradač, M., Gonzalez, A. H., Markevitch, M., Randall, S. W., Jones, C., & Zaritsky, D. *ApJ*, 648, L109 (2006).
17. Springel, V., & Farrar, G. R. *MNRAS*, 380, 911 (2007).
18. Milgrom, M. *ApJ*, 270, 365 (1983).
19. Bekenstein, J. D. *Phys. Rev. D*, 70, 083509 (2004).
20. Zwicky, F. *ApJ*, 86, 217 (1937).
21. Markevitch, M., et al. *ApJ*, 606, 819 (2004).
22. Randall, S. W., et al. *ApJ*, 679, 1173 (2008).
23. Spergel, D. N., & Steinhardt, P. J. *Phys. Rev. Lett.*, 84, 3760 (2000).
24. Takizawa, M. *ApJ*, 520, 514 (1999).
25. Markevitch, M., Govoni, F., Brunetti, G., & Jerius, D. *ApJ*, 627, 733 (2005).
26. Clowe, D., et al., in preparation (2010).
27. Russell, H. R., et al. *MNRAS*, 406, 1721 (2010).
28. Krivonos, R. A., Vikhlinin, A. A., Markevitch, M. L., & Pavlinsky, M. N. *Astronomy Letters*, 29, 425 (2003).
29. Henry, J. P., Finoguenov, A., & Briel, U. G. *ApJ*, 615, 181 (2004).
30. Macario, G., et al., *ApJ*, submitted (2010).
31. Wik, D. R., et al. *ApJ*, 696, 1700 (2009).
32. Ensslin, T. A., Biermann, P. L., Klein, U., & Kohle, S. *A&A*, 332, 395 (1998).
33. Giacintucci, S., et al. *A&A*, 486, 347 (2008).
34. Brunetti, G., et al. *Nature*, 455, 944 (2008).
35. Finoguenov, A., Sarazin, C. L., Nakazawa, K., Wik, D. R., & Clarke, T. E. *ApJ*, 715, 1143 (2010).
36. Mazzotta, P., et al. in preparation (2010).
37. Kang, H., & Jones, T. W. *JKAS*, 35, 159 (2002).
38. Brunetti, G., Setti, G., Feretti, L., & Giovannini, G. *MNRAS*, 320, 365 (2001).
39. Kang, H., & Jones, T. W. *ApJ*, 620, 44 (2005).
40. Kassim, N. E., Clarke, T. E., Enßlin, T. A., Cohen, A. S., & Neumann, D. M. *ApJ*, 559, 785 (2001).
41. Bacchi, M., Feretti, L., Giovannini, G., & Govoni, F. *A&A*, 400, 465 (2003).
42. Liang, H., Hunstead, R. W., Birkinshaw, M., & Andreani, P. *ApJ*, 544, 686 (2000).
43. Govoni, F., Feretti, L., Giovannini, G., Böhringer, H., Reiprich, T. H., & Murgia, M. *A&A*, 376, 803 (2001).

44. Venturi, T., et al. in preparation (2010).
45. Brown, S., & Rudnick, L. *MNRAS*, in press (2010); arXiv:1009.4258
46. Brunetti, G., & Lazarian, A. *MNRAS*, 378, 245 (2007).
47. Miniati, F., Jones, T. W., Kang, H., & Ryu, D. *ApJ*, 562, 233 (2001).
48. Enßlin, T. A. & Gopal-Krishna *A&A*, 366, 26 (2001).